Barrier Heights for Diels-Alder Transition States Leading to Pentacyclic Adducts: A Benchmark Study of Crowded, Strained Transition States of Large Molecules

Maryam Mansoori Kermani, Hanwei Li, Alistar Ottochian, Orlando Crescenzi, Benjamin Janesko, Giovanni Scalmani, Michael Frisch, Ilaria Ciofini, Carlo Adamo, Donald Truhlar

prepared for JPC Lett.

Barrier Heights for Diels-Alder Transition States Leading to Pentacyclic Adducts: A Benchmark Study of Crowded, Strained Transition States of Large Molecules

Maryam Mansoori Kermani,[a] Hanwei Li,[b] Alistar Ottochian,[b] Orlando Crescenzi,[c]
Benjamin G. Janesko,[d] Giovanni Scalmani,[e] Michael J. Frisch,[e]
Ilaria Ciofini,[b] Carlo Adamo,[b,f] and Donald G. Truhlar[a*]

a) *Department of Chemistry, Chemical Theory Center, and Minnesota Supercomputing Institute, University of Minnesota, Minneapolis, Minnesota 55455-0431, USA*
b) *Chimie ParisTech, PSL Research University, CNRS, Institute of Chemistry for Life and Health Sciences, F-75005 Paris, France*
c) *Dipartimento di Scienze Chimiche, Università di Napoli Federico II, Complesso Universitario di Monte Sant'Angelo, Via Cinthia, 80126 Napoli, Italy*
d) *Department of Chemistry & Biochemistry, Texas Christian University, Fort Worth, Texas 76129, USA*
e) *Gaussian, Inc., Wallingford, Connecticut 06492, USA*
f) *Institut Universitaire de France, 103 Boulevard Saint Michel, F-75005 Paris, France*

*corresponding author: truhlar@umn.edu (D.G.T.)

ABSTRACT: Theoretical characterization of reactions of complex molecules depends on providing consistent accuracy for the relative energies of intermediates and transition states. Here we employ the DLPNO-CCSD(T) method with core-valence correlation, large basis sets, and extrapolation to the CBS limit, to provide benchmark values for Diels-Alder transition states leading to competitive strained pentacyclic adducts. We then use those benchmarks to test a diverse set of wave function and density functional methods for the absolute and relative barrier heights of these transition states. Our results show that only a few of the tested density functionals can predict the absolute barrier heights satisfactorily, although relative barrier heights are more accurate. The most accurate functionals tested are ωB97M-V, M11plus, ωB97X-V, PBE-D3(0), M11, and MN15 with MUDs from best estimates less than 3.0 kcal. These findings can guide selection of density functionals for future studies of crowded, strained, transition states of large molecules.

TOC graphic

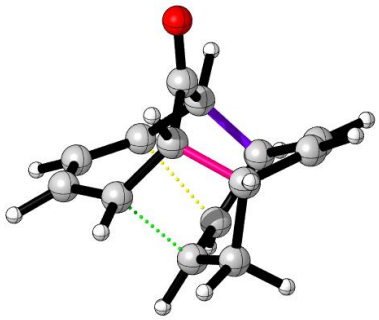

Studies of cycloaddition reactions have a long history.[1,2,3,4,5,6,7,8,9,10,11,12,13,14,15,16,17, 18,19,20] In a recent work, Jamieson et al.[18] studied, among other related reactions, the ambimodal [6+4] cycloaddition of tropone with cycloheptatriene. Key transition states (**TS8** and **TS9**, where we use their numbering for all species, and we put the zero of energy at the overall reactants, as they do) are the transition states for [4+2] Diels-Alder reactions leading from intermediates to the final pentacyclic products, whose structures are **11** and **12**. The reaction steps passing through these transition states are shown in Figure 1. Figure 2 shows the structures of the corresponding transition state **TS8** and **TS9** when viewed from the same direction as Figure 1 and Ref. 18 (Figure S1 in Supporting Information shows the structures of these transition states from other viewing directions). The carbon skeleta of the products, **11** and **12**, are identical, as are the skeletal of the transition structures leading to them and the two reactants. The difference is that the position of the carbonyl group has been exchanged with the only CH_2 in the molecule.

Jamieson et al. obtained best estimates for barrier heights of 9.4 kcal for **TS8** and 14.9 kcal for **TS9**; all energies are relative to the overall reactants (infinitely separated tropone and cycloheptatriene) and are given on a per mole basis. Jamieson et al. noted that transition states, **TS8** and **TS9**, are similarly strained and explained the apparently lower barrier for **TS8** as due to the electronic effect of α,β-unsaturation in its ketone precursor (structure **8**) shown in Figure 1. (That is, the enone in **8** is a better dienophile than the nonconjugated alkene dienophile in **9**.) Upon repeating their calculations with the structures in their Supporting Information (SI), we got a different result, and we started a detailed investigation to understand why. We now understand that they inadvertently switched the labels of **TS8** and **TS9** in the SI.[21] Nevertheless, our study of **TS8** and **TS9** turned out to be very interesting, and we continued to perform a complete theoretical study of the relative energies of these transition states with two objectives: (1) Can we obtain a more accurate best estimate of these barrier heights? (2) What theoretical methods that are practically affordable for large molecules are accurate for predicting the barrier heights of reactions leading to such large, crowded, and strained molecules? We note that this kind of study would have been impossible several years ago, but the ability to calculate high-level best estimates for very large closed-shell singlet molecules made a big leap forward with the development of the DPLNO-CCSD(T) method,[22] and both Jamieson et al. and the present work use this method for best estimates. Our work differs from the previous work in using larger basis sets, including core-valence correlation, and extrapolating to the complete-basis-set (CBS) limit, as well as adding a very broad set of tests of theoretical methods to meet objective 2.

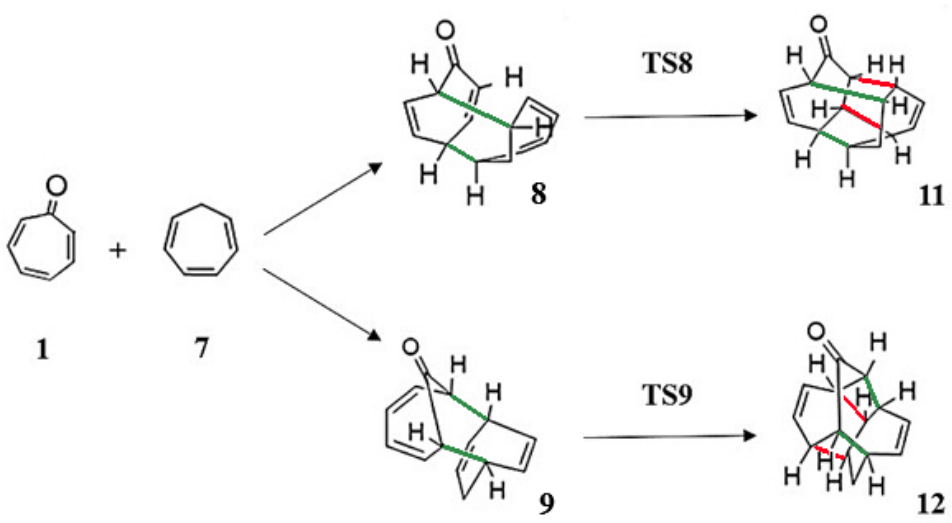

Figure 1. Species **8** and **9** are intermediates produced by reaction of **1** with **7**. The Diels-Alder reactions under study here are passage of **8** through transition state **TS8** to form **11** and passage of **9** through transition state **TS9** to form **12**. The energies in this article are all given with respect to the overall reactants **1** and **7**. Two of the bonds are shown in green to guide the eye from **8** to **11** and from **9** to **12**. The two new single bonds are shown in red.

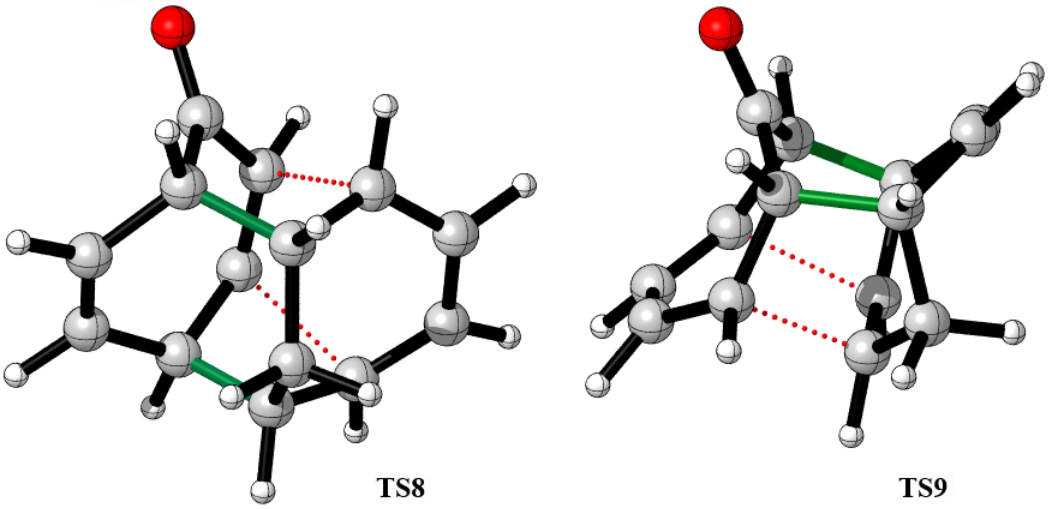

Figure 2. The transition structures. The green bonds are the same as shown in green in **8**, **9**, **11**, and **12** in Figure 1, and the red bonds are the same as shown in red in **11** and **12**. [Color code for ball-and-stick models: O = red, C = gray, and H = white].

To test the accuracy of broadly applicable and newly developed methods, we present calculations by post-Hartree-Fock wave function theory (WFT), leading up to our best estimate, and by density functional theory (DFT) methods. Within DFT methods, we consider calculations both with and without molecular mechanics (i.e., with and without empirical pairwise corrections).

We consider not only the absolute barrier heights ($V^{\ddagger}$), but also the difference in barrier heights, ΔBH, which is a measure of selectivity, and which is defined as $V^{\ddagger}$(**TS9**) minus $V^{\ddagger}$(**TS8**). The barrier height for **TS8** is denoted BH8 and that of **TS9** is denoted BH9. Note that Jamieson et al. specify the heights of the barriers with respect to the overall reactants (**1** + **7**) of the mechanism they studied; therefore, this is a study of the energy of crowded, strained transition states with respect to uncrowded, unstrained species, and that makes it particularly interesting.

Computational details and references for software and basis sets are given at the end in the Computational Details section.

Geometries. Using the exchange-correlation functional MN15-L and the maug-cc-pVTZ basis set (geometries optimized this way are abbreviated //M), we optimized four of the structures shown in Figure 1 – the reactants (**1** and **7**) and **TS8** and **TS9**. The transition states have the chemical formula $C_{14}H_{14}O$. The geometries were similar to those obtained by Jamieson et al. with ωB97X-D/def2-TZVP (abbreviated //ω). Furthermore, high-level WFT calculations (see Table 1) with FC-DLPNO-CCSD(T) with the two largest basis sets yield energy barriers that differ by only 0.4 kcal or less when we compare using //M geometries to using //ω geometries. Therefore, most WFT calculations, including those leading to our best estimate, were carried out at only one geometry. We chose //M for this purpose because the MN15-L exchange-correlation functional is known to generally yield good geometries.[23] For density functional calculations, we use consistently optimized geometries, except for a few cases (labeled "single-point energies") where it is stated otherwise.

WFT calculations and best estimates. The WFT barrier heights and their difference (ΔBH) are shown in Table 1. We show both results with core-valence correlation (denoted all-electron, AE) and results with core electrons uncorrelated (denoted frozen core, FC).

In order to judge the performance of WFT methods, we first obtain a best estimate at the AE level. We will use the complete-basis-set limit (CBS limit) of DPLNO-CCSD(T) calculations for this. This does not include connected quadruple excitations or other higher-order terms, but that is probably not a serious source of error, since Karton[24,25] found that, although beyond-CCSD(T) terms typically raise the calculated barrier for cycloadditions, the increase is usually less than 0.1–0.2 kcal. Furthermore, CCSD(T) is expected to be adequate when the B_1 diagnostic is below 10 kcal (which is an indication that the system or property is not highly multiconfigurational),[26] and we calculated B_1 diagnostics of 5.6 kcal for **TS8** and 5.5 kcal for **TS9**.

To reach the AE complete-basis limit, we employed two-point extrapolation from maug-cc-pCV*x*Z calculations using the formula:[27]

$$E = a + bx^{-3} \qquad (1)$$

where x = 3 and 4 for T and Q, respectively. The result is shown in the table as AE-CBS, and the last column of Table 1 shows the mean unsigned deviation (MUD) of each method from this best estimate.

We also extrapolated FC calculations with the same basis sets, and the results are shown in the table as FC-CBS. We see an error of about 0.3 kcal in MUD due to neglect of core-valence correlation.

Consider next the other calculations, starting with Møller-Plesset second-order perturbation (MP2) calculations. We see large errors with MUDs of 6.4–10.7 kcal and qualitatively incorrect barriers. Coupled cluster theory with single and double excitations (CCSD) reduces the MUDs to 0.4–2.9 kcal. Adding quasiperturbative connected triple excitations [CCSD(T)] calculations with comparable basis sets give errors of 0.4–3.1 kcal. The smaller errors in some of the CCSD calculations compared to CCSD(T) are apparently due in part to cancellation of errors since CCSD(T) calculations with the same basis sets give larger errors. Only when we use DLPNO can we use very large basis sets as required to get the CBS limit. We found that diffuse basis functions have a large effect for smaller basis sets, but our calculations show that the effect is smaller for higher zeta levels.

Table 1. The BH8, BH9, and ΔBH (= BH9 – BH8) energies (kcal) with WFT (post-HF methods

Method	Core//[a]	Basis set[a]	Code[a]	BH8	BH9	ΔBH[a]	MUD[a]
Present work							
MP2	FC//M	MG3S	G	-3.9	2.4	6.3	9.0
MP2	FC//M	6-31+G(d,p)	M	0.0	5.7	5.7	6.4
MP2	FC//M	cc-pVDZ	M	-4.5	1.4	5.9	9.4
MP2	FC//M	maug-cc-pVDZ	G	-2.8	3.1	5.9	8.2
MP2	FC//M	maug-cc-pVDZ	M	-2.8	3.1	5.9	8.2
MP2	FC//M	maug-cc-pVDZ	O	-2.8	3.1	5.9	8.2
MP2	FC//M	maug-cc-pCVDZ	G	-5.7	0.3	6.0	10.2
MP2	FC//M	maug-cc-pVTZ	G	-2.8	3.4	6.3	8.3
CCSD	FC//M	6-31+G(d,p)	M	13.9	18.8	4.9	2.9
CCSD	FC//M	cc-pVDZ	M	10.6	15.6	5.0	0.7
CCSD	FC//M	cc-pVDZ	O	10.6	15.6	5.0	0.7
CCSD	FC//M	maug-cc-pVDZ	M	11.7	16.8	5.0	1.5
CCSD	FC//M	maug-cc-pVDZ	O	11.7	16.8	5.0	1.5
CCSD(T)	FC//M	6-31+G(d,p)	M	10.2	15.0	4.8	0.4
CCSD(T)	FC//M	cc-pVDZ	M	6.6	11.7	5.1	2.2
CCSD(T)	FC//M	cc-pVDZ	O	6.6	11.7	5.1	2.2
CCSD(T)	FC//M	maug-cc-pVDZ	M	7.8	12.8	5.0	1.4
DLPNO-CCSD	FC//M	maug-cc-pVQZ[b]	O	12.4	17.8	5.5	1.9
DLPNO-CCSD	FC//M	maug-cc-pCVQZ[b]	O	12.6	18.0	5.4	2.0
DLPNO-CCSD	FC//M	maug-cc-pCVQZ [c]	O	12.6	18.0	5.4	2.0
DLPNO-CCSD(T)	FC//ω	cc-pVQZ[b]	O	9.4	14.9	5.5	0.1
DLPNO-CCSD(T)	FC//ω	maug-cc-pVQZ[b]	O	9.4	14.9	5.5	0.1
DLPNO-CCSD(T)	FC//M	cc-pVQZ[b]	O	9.0	14.4	5.4	0.4
DLPNO-CCSD(T)	FC//M	maug-cc-pVTZ[d]	O	9.4	14.7	5.3	0.2

DLPNO-CCSD(T)	FC//M	maug-cc-pVQZ[b]	O	9.1	14.5	5.4	0.3
DLPNO-CCSD(T)	FC//M	maug-cc-pCVTZ[c]	O	9.6	14.9	5.3	0.1
DLPNO-CCSD(T)	FC//M	maug-cc-pCVQZ[b]	O	9.3	14.7	5.3	0.2
DLPNO-CCSD(T)	FC//M	maug-cc-pCVQZ[c]	O	9.3	14.7	5.3	0.2
DLPNO-CCSD(T)	FC//M	FC-CBS[e]	O	9.1	14.5	5.4	0.3
MP2	AE//M	cc-pCVTZ	G	-3.4	2.9	6.3	8.6
MP2	AE//M	maug-cc-pCVDZ	G	-6.5	-0.5	6.0	10.7
MP2	AE//M	maug-cc-pCVDZ	O	-6.5	-0.5	6.0	10.7
CCSD	AE//M	cc-pCVDZ	G	9.3	14.4	5.1	0.4
CCSD	AE//M	cc-pCVDZ	O	9.3	14.4	5.1	0.4
CCSD	AE//M	maug-cc-pCVDZ	O	8.9	14.0	5.1	0.6
CCSD(T)	AE//M	cc-pCVDZ	G	5.2	10.3	5.1	3.1
CCSD(T)	AE//M	cc-pCVDZ	O	5.2	10.3	5.1	3.1
DLPNO-CCSD	AE//M	cc-pwCVQZ[f]	O	12.7	18.2	5.4	2.1
DLPNO-CCSD	AE//M	cc-pwCVQZ[g]	O	12.7	18.1	5.4	2.1
DLPNO-CCSD	AE//M	cc-pwCVQZ[c]	O	12.8	18.2	5.4	2.2
DLPNO-CCSD	AE//M	maug- cc-pCVQZ[c]	O	12.8	18.2	5.4	2.2
DLPNO-CCSD	AE//M	maug- cc-pCVQZ[b]	O	12.7	18.2	5.5	2.2
DLPNO-CCSD(T)	AE//M	cc-pCVTZ[d]	O	9.2	14.5	5.3	0.3
DLPNO-CCSD(T)	AE//M	cc-pCVQZ[b]	O	9.4	14.8	5.3	0.1
DLPNO-CCSD(T)	AE//M	cc-pwCVQZ[f]	O	9.5	14.9	5.4	0.0
DLPNO-CCSD(T)	AE//M	cc-pwCVQZ[g]	O	9.5	14.9	5.3	0.1
DLPNO-CCSD(T)	AE//M	cc-pwCVQZ[c]	O	9.6	14.9	5.4	0.1
DLPNO-CCSD(T)	AE//M	maug- cc-pCVTZ[c]	O	9.5	14.9	5.3	0.1
DLPNO-CCSD(T)	AE//M	maug- cc-pCVQZ[c]	O	9.5	14.9	5.4	0.1
DLPNO-CCSD(T)	AE//M	maug- cc-pCVQZ[b]	O	9.5	14.9	5.4	0.0
Best estimate							
DLPNO-CCSD(T)	AE//M	AE-CBS[e]	O	9.5	15.0	5.4	0.0
Refs. 18, 21							
DLPNO-CCSD(T)[c]	FC//ω	cc-pVQZ	O	9.4	14.9	5.5	–

[a] FC//M = frozen core at MN15-L/maug-cc-pVTZ geometries. FC//ω = frozen core at ωB97X-D/def2-TZVP geometries. AE//M = all electrons correlated (aka core-valence correlated) at MN15-L/maug-cc-pVTZ geometries. The basis sets shown in the table are the main basis sets for DPLNO calculations and the auxiliary basis sets are provided in footnotes. G = *Gaussian 16*; O = *ORCA*; M = *Molpro*. The difference BH9 – BH8 was calculated before rounding the numbers to one decimal place. MUD = mean unsigned deviation from best estimates for BH8, BH9, and ΔBH.

[b] The auxiliary basis sets are cc-pVQZ/C and def2/J.

[c] The auxiliary basis sets are cc-pwCVQZ/C and def2/J.

[d] The auxiliary basis sets are cc-pVTZ/C and def2/J.

[e] CBS = complete-basis-set limit obtained by extrapolation (see text). FC-CBS is the complete-basis limit for frozen-core calculations and AE-CBS is the complete-basis limit for all-electron calculations.

[f] Both auxiliary basis sets are replaced by AutoAux.

[g] The auxiliary basis sets are cc-pWCVQZ/C and AutoAux.

The largest calculation in Table 1 is the all-electron calculation with the maug-cc-pCVQZ basis set. This calculation involves 1740 basis functions.

In the final analysis, although our calculations are much more complete than those of Jamieson et al. (they have larger basis sets containing diffuse functions, with core–valence correlation, and with extrapolation to the CBS limit), our best estimates agree well with theirs as seen in the last few rows of Table 1.

It is hard to make an estimate of the reliability of the DLPNO-CCSD(T) results. A previous study of transition state barrier heights[28] concluded that CCSD(T)/CBS is typically about 0.4 kcal from the complete CI limit. Although it is not possible to know in advance whether this error estimate applies to any given reaction, especially when we consider reactions of larger molecules, it does give a rough estimate of the reliability of CCSD(T)/CBS.

However, DLPNO-CCSD(T) involves four thresholds that control the number of electron pairs and other algorithmic cut-offs, and in practical calculations these are set at values for which the DLPNO-CCSD(T) results differ slightly from the canonical CCSD(T) values. We use the defaults threshold that are denoted "NormalPNO", for which the most important threshold is T_{CutPairs} = 1.0E-4 and for which the semicanonical MP2 pair treatment is used. For these choices, the mean deviation in reaction energies from CCSD(T_0) was estimated to be 0.3±0.4 kcal, and the difference of CCSD(T_0) from CCSD(T) was estimated to be on average <0.2 kcal, although they can be much larger in some cases.[29] Compounding these sources of error (0.4, 0.3, and 0.2 kcal) leads to 0.5 kcal estimate for a typical error in reaction energies. Errors in barrier heights for closed -shell transition states (like the present ones) would be expected to be similar or a little larger, and the present systems are also larger (with possibly larger errors) than the systems involved in the benchmarks; furthermore, we use geometries optimized by DFT. Putting all these considerations together, we estimate the accuracy of the best estimates to be 0.5±1 kcal. This is smaller than the typical error in the density functionals for the present problem, so conclusions about density functional accuracy that are drawn from comparison to these best estimates should be valid except when functionals have deviations from the best estimates that are less than 2 kcal.

DFT calculations. Density functional theory is a more practical alternative for widespread applications to large organic molecules, therefore we next consider the applicability of DFT to these barrier heights. Our DFT results are in Table 2.

Table 2. Density functionals tested, their percentage of Hartree-Fock exchange (HFX) and of perturbation theory correlation (PT2), the reference for the functional, the basis set used, the calculated barrier heights (BH8 and BH9), their difference (ΔBH = BH9 – BH8), and the mean unsigned deviation (MUD) of BH8, BH9, and ΔBH from the best estimates (all energies in kcal)

Functional	%HFX[a]	%PT2[a]	Ref.	Basis set	BH8	BH9	ΔBH[b]	MUD
Gradient approximation								
BLYP	0	0	30, 31	MG3S	43.9	50.4	6.5	23.6
				aug-cc-pVTZ	44.3	51.1	6.7	24.1
PBE	0	0	32	aug-cc-pVTZ	18.4	25.7	7.3	7.2
Gradient approximation + molecular mechanics								
PBE-D3(0)	0	0	32	aug-cc-pVTZ	11.6	19.0	7.4	2.7
Gradient approximation + density-based nonlocal correlation								
VV10	0	0	33	aug-cc-pVTZ	19.0	26.0	6.9	7.3
Local meta functional								
M06-L	0	0	34	MG3S	23.9	32.1	8.2	11.4
				aug-cc-pVTZ	23.3	31.2	7.9	10.8
M11-L	0	0	35	aug-cc-pVTZ	20.2	27.8	7.6	8.6
MN15-L	0	0	36	MG3S	18.6	26.7	8.0	7.8
				6-31+G(d,p)	13.3	21.1	7.8	4.1
				maug-cc-pVTZ	17.9	25.9	8.1	7.3
				aug-cc-pVTZ	15.8	23.9	8.1	6.0
revM06-L	0	0	37	MG3S	23.4	31.7	8.2	11.1
				aug-cc-pVTZ	22.8	30.9	8.1	10.6
Meta functional + density-based nonlocal correlation								
B97M-V	0	0	38	aug-cc-pVTZ	17.9	25.4	7.5	7.0
Global hybrid gradient approximation								
B1LYP	25	0	39	MG3S	38.4	44.8	6.5	19.9
B3LYP	20	0	40	MG3S	36.6	43.2	6.6	18.8
				aug-cc-pVTZ	36.9	43.6	6.6	19.1
PBE0	25	0	41	aug-cc-pVTZ	13.8	20.9	7.1	4.0
Global hybrid meta functional								
PW6B95	28	0	42	MG3S	20.8	27.8	7.0	8.6
M06	27	0	43	MG3S	16.2	23.1	6.9	5.4
				aug-cc-pVTZ	16.9	23.7	6.9	5.9
revM06	40.4	0	44	MG3S	15.6	22.6	7.0	5.1
				aug-cc-pVTZ	15.6	22.5	6.9	5.0
MN15	44	0	45	MG3S	13.1	19.8	6.6	3.2
				aug-cc-pVTZ	11.9	18.6	6.6	2.4
M06-2X	54	0	43	aug-cc-pVTZ	13.0	19.5	6.5	3.0
M06-HF	100	0	46	aug-cc-pVTZ	0.7	6.1	5.4	5.9

Global hybrid gradient approximation + molecular mechanics								
B3LYP-D3(0)	20	0	47	MG3S	25.6	32.4	6.8	11.6
				aug-cc-pVTZ	25.7	32.7	6.9	11.8
B3LYP-D3(BJ)	20	0	48	MG3S	21.3	27.7	6.4	8.5
Global hybrid meta functional + molecular mechanics								
PW6B95-D3(0)	28	0	47	MG3S	15.7	22.8	7.2	5.3
PW6B95-D3(BJ)	28	0	28	MG3S	15.3	22.2	7.0	4.9
M06-D3(0)	27	0	49	MG3S	14.2	21.1	6.9	4.1
CF22D	46.2806	0	50	MG3S	13.3	19.9	6.5	3.3
Range-separated hybrid gradient approximation								
CAM-B3LYP	19/65	0	51	aug-cc-pVTZ	26.6	33.0	6.4	12.0
Range-separated hybrid meta functional								
M11	42.8/100	0	52	aug-cc-pVTZ	12.7	19.1	6.4	2.8
M06-SX	33.5/0	0	53	MG3S	16.2	23.5	7.3	5.7
MN12-SX	25/0	0	54	MG3S	19.1	26.3	7.1	7.5
Range-separated hybrid meta functional + rung-3.5 terms								
M11plus	42.8/100	0	55	aug-cc-pVTZ	10.9	16.8	5.9	1.2
Range-separated hybrid gradient approximation + density-based nonlocal correlation								
ωB97X-V	16.7/100	0	56	aug-cc-pVTZ	5.9	12.1	6.2	2.4
Range-separated hybrid meta functional + density-based nonlocal correlation								
ωB97M-V	15/100	0	57	aug-cc-pVTZ	8.7	14.8	6.1	0.6
Range-separated hybrid gradient approximation + molecular mechanics								
ωB97X-D	22/100	0	58	def2-TZVP	12.6	19.4	6.8	3.0
				aug-cc-pVTZ	13.0	19.8	6.8	3.2
Doubly hybrid functional								
B2PLYP	53	27	59	aug-cc-pVTZ	22.4	28.9	6.4	9.3
DSD-PBEP86	68	23/51	60	aug-cc-pVTZ	4.6	10.9	6.3	3.3
PBE-QIDH	69.336	33.333	61	aug-cc-pVTZ	1.1	8.0	6.8	5.6
Doubly hybrid functional + molecular mechanics								
B2PLYP-D3(BJ)	53	27	62	aug-cc-pVTZ	16.5	23.1	6.6	5.4
mPW2PLYP-D	55	25	63	aug-cc-pVTZ	14.3	21.0	6.8	4.1
PBE-QIDH-D3(BJ)	69.336	33.333	64	aug-cc-pVTZ	-1.2	5.6	6.8	7.2
Single-point energies [b]								
B1LYP/MG3S//BLYP/MG3S					38.3	44.9	6.5	20.0
CF22D/MG3S//MN15-L/maug-cc-pVTZ					12.8	19.3	6.5	2.9
PW6B95-D3(0)/MG3S//PW6B95/MG3S					15.7	22.8	7.2	5.3

[a]This is the percentage of Hartree–Fock exchange. For range-separated hybrids and range-separated doubly hybrid functionals, %HFX or %PT2 are shown as A/B, where A is the percentage at small interelectronic separation, and B is the percentage at large interelectronic separation.

[b]The ΔBH values were calculated before rounding the numbers to one decimal place.

[c]Except for the following three rows, all the results in this table are consistently optimized.

Comparing the last three rows of Table 2 to results with consistently optimized geometries shows that the choice of geometry does not have a large effect on our conclusions, and we focus the remaining discussion on the results with consistently optimized geometries.

Table 2 shows results with four polarized-triple-zeta-plus-diffuse-functions basis sets (MG3S, aug-cc-pVTZ, maug-cc-pVTZ, and def2-TZVP) and one basis set that has polarized-double-zeta-plus-diffuse functions (6-31+G(d,p)). The table shows that, even among this diverse batch of basis sets, basis set effects are small, so we may compare calculations with different basis sets without considering basis set effects in detail.

Before comparing the density functional calculations to one another, we compare them to the wave function calculations. Density functional theory with good density functionals is often more accurate than MP2 for barrier heights, a conclusion that is also true for small molecules.[65] However, only the most successful functionals agree reasonably well with CCSD(T) calculations. In particular, 20 of the functionals in Table 2 achieve MUDs smaller than the 6.4 kcal best value achieved by MP2, and eight functionals achieve MUDs smaller than the largest MUD (3.1 kcal) of any of the CCSD(T) calculations. Two functionals (M11plus and ωB97M-V) achieve MUDs in the range 0.6–1.2 kcal.

Table 2 shows very large errors for some of the functionals. For example, BLYP gives an error of ~35 kcal for BH8 and BH9, depending on the basis set. Amazingly, though, all 56 density functional calculations predict ΔBH in the narrow range of 5.4–8.2 kcal, and all except M06-HF, which correctly predicts ΔBH to be 5.4 kcal (although it strongly underestimates absolute barrier heights), predict it in the even narrower range 5.9–8.2 kcal (all off in the same direction, higher than the best estimate). This is even more surprising when one sees that the range of barrier heights predicted for BH8 ranges from –1.2 to 44.3 kcal and that for BH9 ranges from 5.6 to 51.1 kcal. Clearly there is a source of error that is reasonably similar for BH8 and BH9 such that ΔBH is much more accurate than either of the separate barriers. The functionals with nonlocal exchange or correlation tend to predict less difference between the two barriers (and therefore tend to be more accurate for ΔBH) than the local functionals do. Because the distribution of ΔBH predictions is narrow, because the MUD from the best estimate averaged over BH8, BH9, and ΔBH is presented in Table 2 for the reader to examine, and because a functional is considered satisfactory only if it predicts the absolute barrier heights rather than just the ΔBH, the rest of the discussion focusses on just the two absolute barrier heights.

Most of the functionals overestimate the two barrier heights, with overestimates as high as 36 kcal by BLYP, although M06-HF, ωB97X-V, ωB97M-V, DSD-PBEP86, PBE-QIDH, and PBE-QIDH-D3(BJ) underestimate them. The only functionals to have mean signed deviations in the two barrier heights (i.e., now not considering ΔBH) with magnitudes of 4 kcal or less are (alphabetically) DSD-PBEP86, M06-2X, M11, M11plus, MN15, PBE-D3(0), ωB97M-V, ωB97X-D, and ωB97X-V. The next best set of functionals have magnitudes of their mean signed deviations in the range 5–8 kcal and are (again alphabetically) B2PLYP-D3(BJ), M06, M06-SX, MN15-L, mPW2PLYP-D, PBE0, PBE-QIDH, and revM06. The functionals in these lists span a

wide variety of different types and ingredient lists, but the only local functional without molecular mechanics to make it to either of these lists is MN15-L. On average, as usual, the nonlocal functionals give lower (and therefore usually more accurate) barrier heights; the difference is about by ~7–8 kcal (on average), as compared to local functionals. We conclude that adding nonlocality exchange and/or correlation tends to improve the results.

Examination of Table 2 shows categories where functionals with the same ingredients have quite different performance. For example, BLYP and PBE share the same ingredients (but with different functional dependences on these ingredients), but PBE is much more accurate. B1LYP and PBE0 share the same ingredients and even the same percentage of Hartree–Fock exchange, but PBE0 is much more accurate. The popular B3LYP functional, with the same ingredients as B1LYP (although a different percentage of Hartree–Fock exchange) also performs poorly.

Detailed examination of Table 2 shows that one key element in determining the barrier heights is damped dispersion. The local functionals do not predict long-range dispersion, and, in an apparently related failing, many of them underestimate noncovalent interactions even at van der Waals distances where the interaction is not pure dispersion (which is an interaction between subsystems that have no orbital overlap[66]). The nonlocal interaction at van der Waals distances is sometimes called damped-dispersion energy or medium-range correlation energy. The various -D, -D3(0), and -D3(BJ) molecular mechanics terms included in some of the functionals add long-range dispersion and medium-range empirical corrections to the functionals, and this seems to usually improve the barrier heights, in some cases by large amounts. For example, such terms lower the average of BH8 and BH9 by 6.8 kcal for PBE, by 10.9–15.4 kcal for B3LYP, by 5.0–5.6 kcal for PW6B95, by 7.4 kcal for M06, by 5.8 kcal for B2PLYP, and by 2.4 kcal for PBEQIDH. It is noteworthy that this lowering is found even for the B2PLYP and PBEQIDH functionals, which already contain wave-function perturbation theory terms, whose inclusion was motivated in part by the goal of improving dispersion interactions. In the case of PBEQIDH, adding molecular mechanics dispersion makes the results worse, but for the other cases studied, it makes the results better. The improvement of medium-range correlation may also explain why meta functionals tend to do better than gradient approximations. The role of the medium-range correlation energy in improving the barrier heights in reactions of large organic molecules was first discovered in a study of Grubbs catalysts,[67] and the present reactions provide an equally dramatic example.

Another way to include dispersion interactions into density functionals is by density-based nonlocal correlation, as included in VV10, B97M-V, ωB97X-V, and ωB97M-V in Table 2. The mean signed deviations of these four methods for the barrier heights are respectively 10.2, 9.4, –3.2, and −0.5 kcal, so there is no consistent trend showing that this approach provides good accuracy.

Additional comments. The systematic benchmarking of exchange-correlation functionals for individual properties has been instrumental in the establishment of DFT as a method of choice for many applications, including reactivity. Our work complements the conclusions drawn from common benchmark sets involving smaller molecules. The present study is not a comprehensive benchmark; however, it does suggest some general conclusions on the application of approximate electronic structure methods to questions of chemical reactivity. The large molecules studied here

provide a challenging test case in that, among the functionals examined, the average overestimate of the barrier heights is ~9–10 kcal. These large errors illustrate how benchmarking on small molecules does not always indicate the sizes of errors on larger systems. Furthermore, it is possible to obtain very large errors in the barrier heights with MP2 and with some local functionals and global hybrid gradient approximations (that is, global hybrid approximations in which the local part depends on densities and density gradients, but does not contain local kinetic energy density, which is present in global hybrid meta approximations). However, a diverse set of eight functionals yield MUDs on the two barrier heights and the difference in barrier heights (the MUD of Table 2) of 3.3 kcal or less. These most successful functionals have been derived using a variety of criteria and theoretical considerations, illustrating that there is no unique path to improved functionals. An important takeaway from the present study is that the density functionals that do best span a diverse set of functional types, but the functionals that do best include several that might have been expected to do well based on previous work where they are extensively tested on smaller molecules. This indicates some success for the method for developing and testing functionals on systems for which accurate results are available (which are usually smaller systems) and recommending those functionals for applications to more complex systems. But some functionals that did well for smaller test cases do poorly here, illustrating the need for broadening the tests. Additional testing is required to determine the accuracy for predicting the favorability of competing mechanisms of large molecules. It will be interesting to extend the present kind of tests to a broader variety of transition states, such as those in the competing mechanisms in the work of Jamieson et al.

The most accurate density functionals for this problem are (in order) ωB97M-V, M11plus, PBE-D3(0), MN15, M06-2X, ωB97X-D, CF22D, and DSD-PBE86, all of which have an MUD (of two barrier heights and their difference) from our best estimates less than or equal to 3.3 kcal. Alternatively, if one considers the magnitude of the mean signed deviation from the best estimate for only the two absolute barrier heights and uses a magnitude of 4.5 kcal for identifying the most successful functionals, one obtains this same set of functionals plus ωB97X-V and M11. These findings can guide the selection of density functionals for future studies of crowded, strained, transition states of large molecules.

Computational details. We used several software packages: *Gaussian 16,*[68] a locally modified version of *Gaussian 09,*[69,70] the *Gaussian* development version (GDV for M11plus),[71] *Molpro 2019,*[72,73] and *ORCA 4.2.1*.[74,75] We considered several basis sets: 6-31+G(d,p);[76] MG3S[77] (for species containing only H, C, and O, MG3S is the same as 6-311+G(2df,2p)[78]); def2-TZVP;[79] cc-pV*x*Z, aug-cc-pV*x*Z, and maug-cc-pV*x*Z with *x* = D, T, Q;[80,81,82] cc-pCV*x*Z and maug-pCV*x*Z with *x* = D, T, Q;[82,83,84,85,86] and cc-pwCVQZ.[87] The pCV and pwCV basis sets include polarization functions for core-valence correlation in all-electron (AE) calculations, and the other basis sets were developed for frozen-core (FC) calculations. Nevertheless, we use pCV basis sets for some FC calculations to allow a more consistent comparison of FC and AE calculations. Auxiliary basis sets were taken from *ORCA*. Table S4 of the SI shows the keywords that were used for calculations

in *ORCA*. All species are in singlets state, and all calculations are spin restricted. All DFT calculations were done using *Gaussian*, and we used the ultrafine grid (a pruned 99, 590 grid) for them.

ASSOCIATED CONTENT

AUTHOR INFORMATION

Corresponding Author

Donald G. Truhlar − *Department of Chemistry, Chemical Theory Center, and Minnesota Supercomputing Institute, University of Minnesota, Minneapolis, Minnesota 55455-0431, USA;* orcid.org/0000-0002-7742-7294; Email: truhlar@umn.edu

Authors

Maryam Mansoori Kermani − *Department of Chemistry, Chemical Theory Center, and Minnesota Supercomputing Institute, University of Minnesota, Minneapolis, Minnesota 55455-0431, USA;* orcid.org/0000-0002-6715-7796

Hanwei Li – *Chimie ParisTech, PSL Research University, CNRS, Institute of Chemistry for Life and Health Sciences, F-75005 Paris, France*

Alistar Ottochian – *Chimie ParisTech, PSL Research University, CNRS, Institute of Chemistry* for Life and Health Sciences, F-75005 Paris, France

Orlando Crescenzi – *Dipartimento di Scienze Chimiche, Università di Napoli Federico II, Complesso Universitario di Monte Sant'Angelo, Via Cinthia, 80126 Napoli, Italy*

Benjamin G. Janesko – *Department of Chemistry & Biochemistry, Texas Christian University, Fort Worth, Texas 76129, USA*; orcid.org/0000-0002-2572-5273

Giovanni Scalmani – *Gaussian, Inc., Wallingford, Connecticut 06492, USA;* orcid.org/0000-0002-4597-7195

Michael J. Frisch – *Gaussian, Inc., Wallingford, Connecticut 06492, USA*

Ilaria Ciofini – *Chimie ParisTech, PSL Research University, CNRS, Institute of Chemistry for Life and Health Sciences, F-75005 Paris, France.* orcid.org/0000- 0002-5391-4522

Carlo Adamo – *Chimie ParisTech, PSL Research University, CNRS, Institute of Chemistry for Life and Health Sciences, F-75005 Paris, France; Institut Universitaire de France, 103 Boulevard Saint Michel, F-75005 Paris, France;* orcid.org/0000-0002- 2638-2735

Supplementary information

Cartesian coordinates, imaginary frequencies, Hartree-Fock energies, command lines for calculations with *ORCA*, energies of reactants, core-valence correlation energy, additional views of transition states.

Acknowledgments

We appreciate helpful discussions with Pragya Verma. H.L. acknowledges financial support from the China Scholarship Council (grant no. 201908310062). This work was supported in part by the Catalyst Design for Decarbonization Center, an Energy Frontier Research Center, which is funded by the US Department of Energy (DOE), Office of Science, Basic Energy Sciences (BES) under award DE-SC0023383.

References

(1) Hoffmann, R.; Woodward, R. B. Selection Rules for Concerted Cycloaddition Reactions. *J. Am. Chem. Soc.* **1965**, *87*, 2046−2048.

(2) Woodward, R. B.; Hoffmann, R. The Conservation of Orbital Symmetry. *Angew. Chem., Int. Ed. Engl.* **1969**, *8*, 781−853.

(3 Sauer, J.; Sustmann, R. Mechanistic Aspects of Diels-Alder Reactions: A Critical Survey. *Angew. Chem., Int. Ed.* **1980**, *19*, 779-807.

(4) Houk, K. N.; Rondan, N. G.; Mareda, J. Theoretical Studies of Halocarbene Cycloaddition Selectivities. A New Interpretation of Negative Activation Energies and Entropy Control of Selectivity. *Tetrahedron* **1985**, *41*, 1555-1563.

(5) Bernardi, F.; Olivucci, M.; Robb, M. A. Predicting Forbidden and Allowed Cycloaddition Reactions: Potential Surface Topology and its Rationalization. *Acc. Chem. Res.* **1990**, *23*, 405-412.

(6) Corey, E. J. Catalytic Enantioselective Diels-Alder Reactions: Methods, Mechanistic Fundamentals, Pathways, and Applications. *Angew. Chem., Int. Ed.* **2002**, *41*, 1650-1667.

(7) Nicolaou, K. C.; Snyder, S. A.; Montagnon, T.; Vassilikogiannakis, G. The Diels-Alder Reaction in Total Synthesis. *Angew. Chem., Int. Ed.* **2002**, *41*, 1668-1698.

(8) Caramella, P.; Quadrelli, P.; Toma, L. An Unexpected Bispericyclic Transition Structure Leading to 4+2 and 2+4 Cycloadducts in the Endo Dimerization of Cyclopentadiene. *J. Am. Chem. Soc.* **2002**, *124*, 1130−1131.

(9) Agalave, S. G.; Maujan, S. R.; Pore, V. S. Click Chemistry: 1,2,3-Triazoles as Pharmacophores. *Chem. Asian J.* **2011**, *6*, 2696-2718.

(10) Liang, L.; Astruc, D. The Copper(I)-Catalyzed Alkyne-Azide Cycloaddition (CuAAC) "Click" Reaction and its Applications. An overview. *Coord. Chem. Rev.* **2011**, *255*, 2933-2945.

(11) Wang, Y.; Wei, D.; Zhang, W. Recent Advances on Computational Investigations of *N*-Heterocyclic Carbene Catalyzed Cycloaddition/Annulation Reactions: Mechanism and Origin of Selectivities. *ChemCatChem* **2018**, *10*, 338-360.

(12) Houk, K. N.; Liu, F.; Yang, Z.; Seeman, J. I. Evolution of the Diels–Alder Reaction Mechanism Since the 1930s: Woodward, Houk with Woodward, and the Influence of Computational Chemistry on Understanding Cycloadditions. *Angew. Chem., Int. Ed. Engl.* **2021**, *60*, 12660-12681.

(13) Yang, Z.; Dong, X.; Yu, Y.; Yu, P.; Li, Y.; Jamieson, C.; Houk, K. N. Relationships between Product Ratios in Ambimodal Pericyclic Reactions and Bond Lengths in Transition Structures. *J. Am. Chem. Soc.* **2018**, *140*, 3061−3067.

(14) Yu. P.; Chen, T. Q.; Yang, Z.; He, C. Q.; Patel, A.; Lam, Y-H.; Liu, C-Y.; Houk, K. N. Mechanisms and Origins of Periselectivity of the Ambimodal [6 + 4] Cycloadditions of Tropone to Dimethylfulvene. *J. Am. Chem. Soc.* **2017**, *139*, 8251−8258.

(15) Xue, X.-S.; Jamieson, C. S.; Garcia-Borràs, M.; Dong, X.; Yang, Z.; Houk, K. N. Ambimodal Trispericyclic Transition State and Dynamic Control of Periselectivity. *J. Am. Chem. Soc.* **2019**, *141*, 3, 1217–1221.

(16) Roglans, A.; Pla-Quintana, A.; Solà, M. Mechanistic Studies of Transition-Metal-Catalyzed [2 + 2 + 2] Cycloaddition Reactions. *Chem. Rev.* **2021**, *121*, 1894–1979.

(17) Levandowski , B. J.; Raines, R. T. Click Chemistry with Cyclopentadiene. *Chem. Rev.* **2021**, *121*, 6777-6801.

(18) Jamieson, C. S.; Sengupta, A.; Houk, K. N. Cycloadditions of Cyclopentadiene and Cycloheptatriene with Tropones: All Endo-[6+4] Cycloadditions Are Ambimodal. *J. Am. Chem. Soc.* **2021**, *143*, 3918−3926.

(19) Sattarova, A. F.; Biglova, Y. N.; Mustafin, A. G. Quantum-Chemical Approaches in the Study of Fullerene and its Derivatives by the Example of the Most Typical Cycloaddition Reactions: A Review. *Int. J. Quantum Chem.* **2022**, *122*, e26863.

(20) Zhou, Q.; Thøgersen, M. K.; Rezayee, N. M.; Jørgensen, K. A.; Houk, K. N.; Ambimodal Bispericyclic [6 + 4]/[4 + 6] Transition State Competes with Diradical Pathways in the Cycloheptatriene Dimerization: Dynamics and Experimental Characterization of Thermal Dimers. *J. Am. Chem. Soc.* **2022**, *144*, 22251−22261.

(21) Jamieson, C. S.; Sengupta, A.; Houk, K. N. Correction to "Cycloadditions of Cyclopentadiene and Cycloheptatriene with Tropones: All Endo-[6+4] Cycloadditions Are Ambimodal." *J. Am. Chem. Soc.* **2023,** *145*, 9366.

(22) Guo, Y.; Riplinger, C.; Becker, U.; Liakos, D. G.; Minenkov, Y.; Cavallo, L.; Neese, F. Communication: An Improved Linear Scaling Perturbative Triples Correction for the Domain Based Local Pair-Natural Orbital Based Singles and Doubles Coupled Cluster Method [DLPNO-CCSD(T)]. *J. Chem. Phys.* **2018**, *148*, 011101.

(23) Verma, P.; Truhlar, D. G. Status and Challenges of Density Functional Theory. *Trends in Chemistry* **2020**, *2*, 302−318.

(24) Karton, A. Highly Accurate CCSDT(Q)/CBS Reaction Barrier Heights for a Diverse Set of Transition Structures: Basis Set Convergence and Cost-Effective Approaches for Estimating Post-CCSD(T) Contributions. *J. Phys. Chem. A* **2019**, *123*, 6720–6732.

(25) Kozuch, S.; Schleif, T.; Karton, A. Quantum Mechanical Tunnelling: The Missing Term to Achieve Sub-kJ/mol Barrier Heights. *Phys. Chem. Chem. Phys.* **2021**, *23*, 10888–10898.

(26) Schultz, N. E.; Zhao, Y.; Truhlar, D. G. Density Functionals for Inorganometallic and Organometallic Chemistry. *J. Phys. Chem. A* **2005**, *109*, 11127−11143.

(27) Helgaker, T.; Klopper, W.; Koch, H.; Noga, J. Basis-Set Convergence of Correlated Calculations on Water. *J. Chem. Phys.* **1997**, *106*, 9639–9646.

(28) Papajak, E.; Truhlar, D. G. What are the Most Efficient Basis Set Strategies for Correlated Wave Function Calculations of Reaction Energies and Barrier Heights? *J. Chem. Phys.* **2012**, *137*, 1−8.

[29] Liakos, D. G.; Sparta, M.; Kesharwani, M. K.; Martin, J. M. L.; Neese, F. Exploring the Accuracy Limits of Local Pair Natural Orbital Coupled-Cluster Theory. *J. Chem. Theory Comput.* **2015**, *11*, 1525−1539.

(30) Becke, A. D. Density-Functional Exchange-Energy Approximation with Correct Asymptotic-Behavior. *Phys. Rev. A* **1988**, *38*, 3098-3100.

(31) Lee, C.; Yang, W.; Parr, R. G. Development of the Colle-Salvetti Correlation-Energy Formula into a Functional of the Electron Density. *Phys. Rev. B* **1988**, *37*, 785–789.

(32) Perdew, J. P.; Burke, K.; Ernzerhof, M. Generalized Gradient Approximation Made Simple. *Phys. Rev. Lett.* **1996**, *77*, 3865–3868.

(33) Vydrov, O. A.; Van Voorhis, T. Nonlocal van der Waals Density Functional: The Simpler the Better. *J. Chem. Phys.* **2010**, *133*, 244103.

(34) Zhao, Y.; Truhlar, D. G. A New Local Density Functional for Main-group Thermochemistry, Transition Metal Bonding, Thermochemical Kinetics, and Noncovalent Interactions. *J. Chem. Phys.* **2006**, *125*, 194101.

(35) Peverati, R.; Truhlar, D. G. M11-L: A Local Density Functional That Provides Improved Accuracy for Electronic Structure Calculations in Chemistry and Physics. *J. Phys. Chem. Lett.* **2012**, *3*, 117–124.

(36) Yu, H. S.; He X.; Truhlar, D. G. MN15-L: A New Local Exchange-Correlation Functional for Kohn–Sham Density Functional Theory with Broad Accuracy for Atoms, Molecules, and Solids. *J. Chem. Theory Comput.* **2016**, *12*, 1280-1293.

(37) Wang, Y.; Jin, X.; Yu, H. S.; Truhlar, D. G.; He, X. Revised M06-L Functional for Improved Accuracy on Chemical Reaction Barrier Heights, Noncovalent Interactions, and Solid-State Physics. *Proc. Nat. Acad. Sci. USA* **2017**, *114*, 8487-8492.

(38) Mardirossian, N.; Head-Gordon, M. Mapping the Genome of Meta-Generalized Gradient Approximation Density Functionals: The Search for B97M-V. *J. Chem. Phys.* **2015**, *142*, 074111.

(39) Adamo, C.; Barone, V. Toward Reliable Adiabatic Connection Models Free from Adjustable Parameters. *Chem. Phys. Lett.* **1997**, *274*, 242-250.

(40) Stephens, P. J.; Devlin, F. J.; Chabalowski, C. F.; Frisch, M. J. Ab Initio Calculation of Vibrational Absorption and Circular Dichroism Spectra Using Density Functional Force Fields. *J. Phys. Chem.* **1994**, *98*, 11623–11627.

(41) Adamo, C.; Barone, V. Toward Reliable Density Functional Methods without Adjustable Parameters: The PBE0 Model. *J. Chem. Phys.* **1999**, *110*, 6158–6170.

(42) Zhao, Y.; Truhlar, D. G. Design of Density Functionals That Are Broadly Accurate for Thermochemistry, Thermochemical Kinetics, and Nonbonded Interactions, *J. Phys. Chem. A* **2005**, *109*, 5656-5667.

(43) Zhao, Y.; Truhlar, D. G. The M06 Suite of Density Functionals for Main Group Thermochemistry, Thermochemical Kinetics, Noncovalent Interactions, Excited States, and Transition Elements: Two New Functionals and Systematic Testing of Four M06-class Functionals and 12 other Functionals. *Theor. Chem. Acc.* **2008**, *120*, 215-241.

(44) Wang, Y.; Verma, P.; Jin, X.; Truhlar, D. G.; He, X. Revised M06 Density Functional for Main-Group and Transition-Metal Chemistry. *Proc. Nat. Acad. Sci. USA* **2018**, *115*, 10257-10262.

(45) Yu, H. S.; He, X.; Li, S. L.; Truhlar, D. G. MN15: A Kohn–Sham Global-Hybrid Exchange–Correlation Density Functional with Broad Accuracy for Multi-Reference and Single-Reference Systems and Noncovalent Interactions. *Chem. Sci.* **2016**, *7*, 5032-5051.

(46) Zhao, Y.; Truhlar, D. G. Density Functional for Spectroscopy: No Long-Range Self-Interaction Error, Good Performance for Rydberg and Charge-Transfer States, and Better Performance on Average than B3LYP for Ground States. *J. Phys. Chem. A* **2006**, *110*, 13126–13130.

(47) Grimme, S.; Antony, J.; Ehrlich, S.; Krieg, H. A Consistent and Accurate Ab Initio Parametrization of Density Functional Dispersion Correction (DFT-D) for the 94 elements H-Pu. *J. Chem. Phys.* **2010**, *132*, 154104.

(48) Grimme, S.; Antony, J.; Ehrlich, S.; Goerigk, L. Effect of the Damping Function in Dispersion Corrected Density Functional Theory. *J. Comput. Chem.* **2011**, *32*, 1456–1465.

(49) Goerigk, L.; Grimme, S. A Thorough Benchmark of Density Functional Methods for General Main Group Thermochemistry, Kinetics, and Noncovalent Interactions. *Phys. Chem. Chem. Phys.* **2011**, *13*, 6670–6688.

(50) Liu, Y.; Zhang, C.; Liu, Z.; Truhlar, D. G.; Wang, Y.; He, X. Supervised Learning of a Chemistry Functional with Damped Dispersion. *Nat. Comput. Sci.* **2023**, *3*, 48-58.

(51) Yanai, T.; Tew, D. P.; Handy, N. C. A New Hybrid Exchange–Correlation Functional Using the Coulomb-Attenuating Method (CAM-B3LYP). *Chem. Phys. Lett.* **2004**, *393*, 51–57.

(52) Peverati, R.; Truhlar, D. G. Improving the Accuracy of Hybrid Meta-GGA Density Functionals by Range Separation. *J. Phys. Chem. Lett.* **2011**, *2*, 2810–2817.

(53) Wang, Y.; Verma, P.; Zhang, L.; Li, Y.; Liu., Z.; Truhlar, D. G.; He, X. M06-SX Screened-Exchange Density Functional for Chemistry and Solid-State Physics. *Proc. Nat. Acad. Sci. USA* **2020**, *117*, 2294-2301.

(54) Peverati, R.; Truhlar, D. G. Screened-exchange Density Functionals with Broad Accuracy for Chemistry and Solid-State physics. *Phys. Chem. Chem. Phys.* **2012**, *14*, 16187–16191.

(55) Verma, P.; Janesko, B. G.; Wang, Y.; He, X.; Scalmani, G.; Frisch, M. J.; Truhlar, D. G. M11plus: A Range-Separated Hybrid Meta Functional with Both Local and Rung-3.5 Correlation Terms and High Across-the-Board Accuracy for Chemical Applications. *J. Chem. Theory Comput.* **2019**, *15*, 4804–4815.

(56) Mardirossian, N.; Head-Gordon, M. ωB97X-V: A 10-Parameter, Range-Separated Hybrid, Generalized Gradient Approximation Density Functional with Nonlocal Correlation, Designed by a Survival-of-the-Fittest Strategy. *Phys. Chem. Chem. Phys.* **2014**, *16*, 9904-9924.

(57) Mardirossian, N.; Head-Gordon, M. ωB97M-V: A Combinatorially Optimized, Range-Separated Hybrid, Meta-GGA Density Functional with VV10 Nonlocal Correlation. *J. Chem. Phys.* **2016**, *144*, 214110.

(58) Chai, J.-D.; Head-Gordon, M. Long-range Corrected Hybrid Density Functionals with Damped Atom–Atom Dispersion Corrections. *Phys. Chem. Chem. Phys.* **2008**, *10*, 6615-6620.

(59) Grimme, S. Semiempirical Hybrid Density Functional with Perturbative Second-Order Correlation. *J. Chem. Phys.* **2006**, *124*, 034108.

(60) Kozuch, S.; Martin, J. M. L. DSD-PBEP86: In Search of the Best Double-Hybrid DFT with Spin-Component Scaled MP2 and Dispersion Corrections. *Phys. Chem. Chem. Phys.* **2011**, *13*, 20104-20107.

(61) Brémond, É.; Sancho-García, J. C.; Pérez-Jiménez, Á. J.; Adamo, C. Communication: Double-Hybrid Functionals from Adiabatic-Connection: The QIDH Model. *J. Chem. Phys.* **2014**, *141*, 031101.

(62) Schwabe, T.; Grimme, S. Double-Hybrid Density Functionals with Long-Range Dispersion Corrections: Higher Accuracy and Extended Applicability. *Phys. Chem. Chem. Phys.* **2007**, *9*, 3397-3406.

(63) Huenerbein, R.; Schirmer, B.; Moellmann, J.; Grimme, S. Effects of London Dispersion on the Isomerization Reactions of Large Organic Molecules: A Density Functional Benchmark Study. *Phys. Chem. Chem. Phys.* **2010**, *12*, 6940–6948.

(64) Sancho-García, J. C.; Brémond, É.; Savarese, M.; Pérez-Jiménez, A. J.; Adamo, C. Partnering Dispersion Corrections with Modern Parameter-Free Double-Hybrid Density Functionals. *Phys. Chem. Chem. Phys.*, **2017**, *19*, 13481-13487.

(65) Zheng, J.; Zhao, Y.; Truhlar, D. G. The DBH24/08 Database and Its Use to Assess Electronic Structure Model Chemistries for Chemical Reaction Barrier Heights. *J. Chem. Theory Comput.* **2009**, *5*, 808-821.

(66) Truhlar, D. G. Dispersion Forces − Neither Fluctuating nor Dispersing, *J. Chem. Educ.* **2019**, *96*, 1671−1675.

(67) Zhao, Y.; Truhlar, D. G. A Density Functional Theory that Accounts for Medium-Range Correlation Energies in Organic Chemistry. *Org. Lett.* **2006**, *8*, 5753-5755.

(68) Frisch, M. J. et al. *Gaussian 16*, revision C.01; Gaussian, Inc.: Wallingford, CT, 2016.

(69) Frisch, M. J. et al. *Gaussian 09*, revision C.01; Gaussian, Inc.: Wallingford, CT, 2009.

(70) Zhao, Y.; Peverati, R.; Yang, K. R.; Luo, S.; Yu, H. S.; He, X.; Wang, Y.; Verma, P.; Truhlar, D. G. *MN-GFM*, version 6.10: Minnesota–Gaussian Functional Module. http://comp.chem.umn.edu/mn-gfm (accessed Aug. 10, 2018).

(71) Frisch, M. J.; Trucks, G. W.; Schlegel, H. B.; Scuseria, G. E.; Robb, M. A.; Cheeseman, J. R.; Scalmani, G.; Barone, V.; Petersson, G. A.; Nakatsuji, H.; Li, X.; Caricato, M.; Marenich, A. V.; Bloino, J.; Janesko, B. G.; Gomperts, R.; Mennucci, B.; Hratchian, H. P.; Ortiz, J. V.; Izmaylov, A. F.; Sonnenberg, J. L.; Williams-Young, D.; Ding, F.; Lipparini, F.; Egidi, F.; Goings, J.; Peng, B.; Petrone, A.; Henderson, T.; Ranasinghe, D.; Zakrzewski, V. G.; Gao, J.; Rega, N.; Zheng, G.; Liang, W.; Hada, M.; Ehara, M.; Toyota, K.; Fukuda, R.; Hasegawa, J.; Ishida, M.; Nakajima, T.; Honda, Y.; Kitao, O.; Nakai, H.; Vreven, T.; Throssell, K.; Montgomery, J. A., Jr.; Peralta, J. E.; Ogliaro, F.; Bearpark, M. J.; Heyd, J. J.; Brothers, E. N.; Kudin, K. N.; Staroverov, V. N.; Keith, T. A.; Kobayashi, R.; Normand, J.; Raghavachari, K.; Rendell, A. P.; Burant, J. C.; Iyengar, S. S.; Tomasi, J.; Cossi, M.; Millam, J. M.; Klene, M.; Adamo, C.; Cammi, R.; Ochterski, J. W.; Martin, R. L.; Morokuma, K.; Farkas, O.; Foresman, J. B.; Fox, D. J. *Gaussian Development Version* Revision I.14+, Gaussian, Inc., Wallingford CT, 2018.

(72) Werner, H.-J.; Knowles, P. J.; Knizia, G.; Manby, F. R.; Schütz M. Molpro: A General-Purpose Quantum Chemistry Program Package. *WIREs Comput. Mol. Sci.* **2012**, *2*, 242-253.

(73) Werner, H.-J. et al. The Molpro Quantum Chemistry Package. *J. Chem. Phys.* **2020**, *152*, 144107.

(74) Neese, F. The ORCA Program System. *WIREs Comput. Mol. Sci.* **2012**, *2*, 73–78.

(75) Neese, F. Software Update: The ORCA Program System, Version 4.0. *WIREs Comput. Mol. Sci.* **2018**, *8*, e1327.

(76) Francl, M. M.; Pietro, W. J.; Hehre, W. J.; Binkley, J. S.; DeFrees, D. J.; Pople, J. A.; Gordon, M. S. Self-Consistent Molecular Orbital Methods. 23. A Polarization-Type Basis Set for 2nd-Row Elements. *J. Chem. Phys.* **1982**, *77*, 3654-3665.

(77) Lynch, B. J.; Zhao, Y.; Truhlar, D. G. Effectiveness of Diffuse Basis Functions for Calculating Relative Energies by Density Functional Theory. *J. Phys. Chem. A* **2003**, *107*, 1384−1388.

(78) Raghavachari, K.; Binkley, J. S.; Seeger, R.; Pople, J. A. Self-Consistent Molecular Orbital Methods. 20. Basis Set for Correlated Wave-Functions. *J. Chem. Phys.* **1980**, *72*, 650-654.

(79) Weigend, F.; Ahlrichs, R. Balanced Basis Sets of Split Valence, Triple Zeta Valence and Quadruple Zeta Valence Quality for H to Rn: Design and Assessment of Accuracy. *Phys. Chem. Chem. Phys.* **2005**, *7*, 3297-3305.

(80) Dunning, T. H. Jr. Gaussian Basis Sets for Use in Correlated Molecular Calculations. I. The Atoms Boron through Neon and Hydrogen. *J. Chem. Phys.* **1989**, *90*, 1007-1023.

(81) Kendall, R. A.; Dunning, T. H.; Harrison, R. J. Electron Affinities of the First-Row Atoms Revisited. Systematic Basis Sets and Wave Functions. *J. Chem. Phys.* **1992**, *96*, 6796−6806.

(82) Papajak, E.; Zheng, J.; Xu, X.; Leverentz, H. R.; Truhlar, D. G. Perspectives on Basis Sets Beautiful: Seasonal Plantings of Diffuse Basis Functions. *J. Chem. Theory Comput.* **2011**, *7*, 10, 3027–3034.

(83) Schuchardt, K. L.; Didier, B. T.; Elsenthagen, T.; Sun, L.; Gurumoorthi, V.; Chase, J.; Li, J.; Windus, T. L. Basis Set Exchange: A Community Database for Computational Sciences. *J. Chem. Inf. Model.* **2007**, *47*, 1045-1052.

(84) Feller, D. The Role of Databases in Support of Computational Chemistry Calculations. *J. Comput. Chem.* **1996**, *17*, 1571-1586.

(85) Pritchard, B., P.; Altarawy, D.; Didier, B.; Gibson, T. D.; Windus, T. L. New Basis Set Exchange: An Open, Up-to-Date Resource for the Molecular Sciences Community. *J. Chem. Inf. Model.* **2019**, *59*, 4814-4820.

(86) Woon, D. E.; Dunning, T. H. Jr. Gaussian Basis Sets for Use in Correlated Molecular Calculations. V. Core-Valence Basis Sets for Boron through Neon. *J. Chem. Phys.* **1995**, *103*, 4572-4585.

(87) Peterson, K. A.; Dunning, T. H. Jr. Accurate Correlation Consistent Basis Sets for Molecular Core–Valence Correlation Effects: The Second Row Atoms Al–Ar, and the First Row Atoms B–Ne Revisited. *J. Chem. Phys.* **2002**, *117*, 10548-10560.